Ion specific correlations in bulk and at biointerfaces

2009 J. Phys.: Condens. Matter 21 424108

(http://iopscience.iop.org/0953-8984/21/42/424108)

IOP Publishing Journal of Physics: Condensed Matter

J. Phys.: Condens. Matter **21** (2009) 424108 (10pp) doi:10.1088/0953-8984/21/42/424108

Ion specific correlations in bulk and at biointerfaces

I Kalcher, D Horinek, R R Netz and J Dzubiella[1]

Physics Department T37, Technical University Munich, 85748 Garching, Germany

E-mail: jdzubiel@ph.tum.de

Received 29 March 2009
Published 29 September 2009
Online at stacks.iop.org/JPhysCM/21/424108

Abstract

Ion specific effects are ubiquitous in any complex colloidal or biological fluid in bulk or at interfaces. The molecular origins of these 'Hofmeister effects' are not well understood and their theoretical description poses a formidable challenge to the modeling and simulation community. On the basis of the combination of atomistically resolved molecular dynamics (MD) computer simulations and statistical mechanics approaches, we present a few selected examples of specific electrolyte effects in bulk, at simple neutral and charged interfaces, and on a short α-helical peptide. The structural complexity in these strongly Coulomb-correlated systems is highlighted and analyzed in the light of available experimental data. While in general the comparison of MD simulations to experiments often lacks quantitative agreement, mostly because molecular force fields and coarse-graining procedures remain to be optimized, the consensus as regards trends provides important insights into microscopic hydration and binding mechanisms.

(Some figures in this article are in colour only in the electronic version)

1. Introduction

Aqueous electrolytes are of fundamental importance to physical chemistry, biology, and the evolution and function of life. In particular, the simple ions Na^+, K^+, and Cl^- are significant ingredients in the specific or unspecific regulation of (bio)molecular processes, such as action potentials, osmotic flows, and the stabilization and function of proteins, lipids, and nucleic acids [1]. The specific action of individual ions (e.g., Na^+ versus K^+ or Cl^- versus I^-) has received increased attention recently and triggered a revival in the investigation of ionic properties in bulk, at interfaces, and in their action on biomolecules and accompanying 'Hofmeister effects' [2–6]. The latter terminology, referring to Hofmeister's investigation of salt's individual action on the precipitation of egg white lysozyme [7], is often used synonymously for ion specific effects in complex fluids; typically those are found categorized in cation and anion 'Hofmeister series' but are not unique in general.

Even in homogeneous bulk electrolytes, salt specificity occurs already at electrolyte concentrations ρ larger than the Debye–Hückel limiting value of $\simeq$10 mM [8] and affects macroscopic quantities, such as the solution activity, the electrolyte osmotic pressure Π, and the static dielectric constant $\epsilon(\rho)$. These experimentally accessible properties exhibit nontrivial trends and a complex dependence on salt concentration and type. The osmotic pressure at concentration ρ, for instance, is larger for NaCl when compared to KCl, but the order is reversed if F^- is the cation [9]. Similarly, the interface thermodynamics expressed for example in terms of adsorption, interfacial tension, or pressure (interaction) between confining biological surfaces shows a sensitive dependence on salt type [6, 10]. Consequently, macromolecule (protein) structure, solubilities, and virial coefficients show significant salt specificity [4, 11]. The microscopic reason for the latter lies apparently in the complex hydration structure around individual or interacting (bulk and surface) groups in the aqueous environment [10, 12–14]. The competition of the strong and long-ranged Coulombic interactions, which governs spatial correlations and the structure of the hydrogen bond network at short scales, makes the theoretical prediction of microscopic and integrated macroscopic quantities quite a challenging task.

In principle, a means to access the detailed solution structure is provided by classical molecular dynamics (MD) computer simulations [15–23] in which water atoms and ions are explicitly resolved by assigning (partial) Coulombic point charges q_i, excluded volume sizes, and dispersion attractions.

[1] Author to whom any correspondence should be addressed.

Typically the nonelectrostatic atom–atom interaction between atom i and j in a distance r_{ij} is modeled by a Lennard-Jones (LJ) interaction of the form

$$V_{\mathrm{LJ}}(r_{ij}) = 4\epsilon_{ij}\left[\left(\frac{\sigma_{ij}}{r_{ij}}\right)^{12} - \left(\frac{\sigma_{ij}}{r_{ij}}\right)^{6}\right], \tag{1}$$

where σ_{ij} is the interaction length and ϵ_{ij} determines the energy scale. The whole set $\{\sigma, \epsilon, q\}$ accompanied by adequate mixing rules typically defines the total *force field* behind the intermolecular MD interactions. For water, usually simple point charge models (e.g., SPC or SPC/ E) are used in which oxygen and hydrogen atoms are resolved [24]. The latter are connected by rigid intramolecular bonds and carry partial charges optimized such that a few important water properties (density, structure, surface tension, dielectric constant) are well reproduced. The empirical force fields for the ions, however, are typically benchmarked to single-ion properties, such as the solvation free energy, and often fail to reproduce realistic electrolyte structure or thermodynamics at nonvanishing concentrations. As has been recognized in early literature, there is a strong sensitivity of electrolyte thermodynamics to small changes in the potential of mean force between the interacting ionic constituents [25–27]. Ion force field development thus still remains an active field of research [28–30] and quantitative statements have to be considered and checked carefully. Many recent MD simulations that are in quantitative or qualitative agreement with experimental trends, however, have clearly deepened molecular insight on ion specific interactions in physical chemistry and biology; see e.g., [2, 3, 5, 7, 31–36] and references therein.

On the basis of atomistic MD computer simulations and statistical mechanics approaches, in this work we present a few selected examples of specific electrolyte effects in bulk, at simple interfaces, and on the structural stability of a small biomolecule. The structural complexity in these strongly Coulomb-correlated systems is highlighted and interpreted in the light of available experimental data. Parts of this work have been published elsewhere [5, 37].

In the first section we exemplify the intimate connection between the water-mediated electrolyte structure, electrolyte-induced water polarization, and ion specific thermodynamics in homogeneous bulk solutions. In section 3 we present original results of ion adsorption at simple neutral and charged interfaces and discuss possible effects on surface tension and interfacial interactions. The last section is devoted to a more biological system and illustrates the action of specific ions on the stability and denaturation of a single α-helical peptide in which a combination of subtle binding effects play a role. We briefly conclude in section 5.

2. Ion specific bulk correlations and thermodynamics

The structure of homogeneous electrolyte solutions with concentration ρ is typically expressed in terms of radial distribution functions (rdfs) $g_{ij}(r;\rho)$ between a pair of ions i and j. The corresponding potential of mean force (pmf) is obtained by a Boltzmann inversion [38, 39] and reads

$$\beta w_{ij}(r;\rho) = -\ln[g_{ij}(r;\rho)], \tag{2}$$

where $\beta^{-1} = k_{\mathrm{B}}T$ is the thermal energy. It is instructive for the analysis of charged systems to decompose the pmf into short-ranged and long-ranged contributions via [22, 23, 40, 41]

$$w_{ij}(r;\rho) = w_{ij}^{\mathrm{sr}}(r;\rho) + w_{ij}^{\mathrm{DH}}(r;\rho), \tag{3}$$

where the short-ranged part $w_{ij}^{\mathrm{sr}}(r;\rho)$ can be assumed independent of ρ for dilute systems below a typical overlap concentration $\rho \lesssim 0.5$ M [37]. The long-ranged part in (3) is typically approximated by a Debye–Hückel (DH) type of potential [8, 40] of the form

$$\beta w_{ij}^{\mathrm{DH}}(r;\rho) = \lambda_{ij}(\rho)\exp[-\kappa(\rho)r]/r, \tag{4}$$

which is strictly valid only for infinitely dilute electrolyte systems [40]. In a more general sense, equation (3) in combination with equation (4) can be viewed as a definition of the short-ranged potential $w_{ij}^{\mathrm{sr}}(r)$. In equation (4), $\lambda_{ij}(\rho)$ is an *a priori* unknown prefactor with the unit of length. For symmetric, monovalent electrolytes the inverse screening or Debye length is $\kappa(\rho) = [8\pi\lambda_{\mathrm{B}}(\rho)\rho]^{1/2}$ and the electrostatic coupling parameter called the Bjerrum length is defined as $\lambda_{\mathrm{B}}(\rho) = \beta e^2/[4\pi\epsilon_0\epsilon(\rho)]$. These material equations become exact in the asymptotic low concentration limit. At finite concentration, the Bjerrum length acquires an implicit dependence on ρ due to the salt-induced change of the (static) water dielectric constant $\epsilon(\rho)$ [10]. In principle, this could also be interpreted as charge renormalization [42]. In the low density limit of the salt ($\rho \to 0$), the pmf between two ions reduces to their mutual effective *pair potential* $V_{ij}(r) = \lim_{\rho\to 0} w_{ij}(r;\rho)$, which consists of the intrinsic (vacuum) ion–ion interaction and the *water-mediated contribution*. The pmf decomposition (3) is then identical to splitting the pair potential into a short-ranged and a pure Coulombic part as given by

$$V_{ij}(r) = V_{ij}^{\mathrm{sr}}(r) + \lambda_{\mathrm{B}}(0)/r. \tag{5}$$

By utilizing the empirical fact that the short-ranged part w_{ij}^{sr} is density independent for small but nonzero concentrations, the unknown Debye–Hückel prefactor $\lambda_{ij}(\rho)$ can be quantified as described in detail in [37]. Thus, the long-ranged Debye–Hückel part of the interaction can be subtracted from $w_{ij}(r;\rho)$ to obtain the short-ranged pair potential via

$$V_{ij}^{\mathrm{sr}} = w_{ij}^{\mathrm{sr}}(r;\rho) = w_{ij}(r;\rho) - w_{ij}^{\mathrm{DH}}(r;\rho), \tag{6}$$

where the left-hand side is valid for $\rho \lesssim 0.5$ M [37]. The total pair potential $V_{ij}(r)$ at infinite dilution then follows from equation (5).

Figure 1 shows anion–cation short-ranged potentials for the salts LiCl, NaCl, KCl, CsCl, and NaI derived from $\simeq$100 ns long, explicit-water bulk MD simulations using the SPC/ E water model and nonpolarizable ions [37]. Dang's ion force field is used [43–45]; see table 1. Recall that those short-ranged potentials include all interactions except the Coulomb or Debye–Hückel interaction which has been

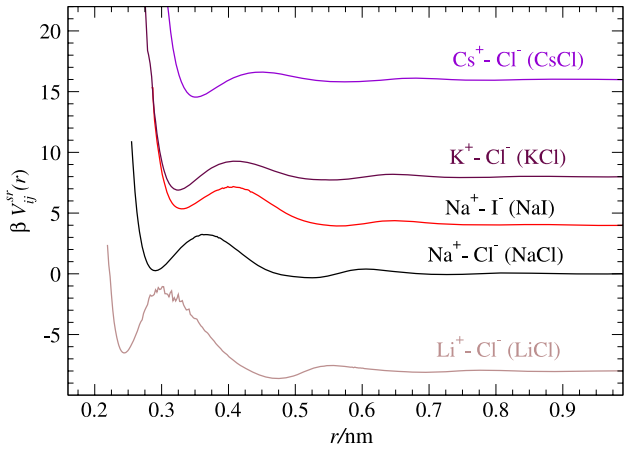

Figure 1. (Color online) Infinite-dilution short-ranged pair potential $V_{ij}^{\mathrm{sr}}(r;\rho)$ between anions and cations versus their distance r obtained from explicit-water MD simulations [37]. The curves are shifted by a constant for better comparison.

separated out. As such, the potentials mainly reflect the distance-dependent mutual perturbation of the ionic hydration shells. All potentials show a steep increase at contact which stems from the repulsive part of the LJ interaction built into the simulation model, while the contact distance, i.e., the location of the first minimum, increases with increasing bare ion size. For example, for the chloride salts the contact distance increases in the order LiCl < NaCl < KCl < CsCl. All potentials show two local minima, one minimum at contact and a second minimum corresponding to a solvent-separated ion pair. For some potentials even a third local minimum is discernible, which corresponds to two ions that are each surrounded by a complete hydration shell. The ion pairs LiCl, NaI, and NaCl show the most favorable interaction at the second, solvent-separated minimum. For the larger potassium and cesium ions the situation is reversed and the primary minimum corresponding to an ion pair in direct contact is preferred. Apparently, the rather size-symmetric ions (i.e., with a comparable LJ parameter σ_{ij}) form contact ion pairs, while the size-asymmetric pairs prefer the solvent-separated configuration. It has been argued that this 'like likes like' behavior is a general trend originating in matching of water affinities of similarly sized ions [46–48].

This picture suggests that the more size-symmetric ion pairs such as KCl or CsCl may exhibit stronger attraction in solution than the size-asymmetric salts LiCl and NaI. This local argument should also have a bearing on integral thermodynamic properties such as osmotic coefficients, activity coefficients, maximal solubilities or heats of solution. A convenient approach to thermodynamics is provided by the *virial route* where the osmotic coefficient $\phi(\rho) = \Pi/(2\rho k_{\mathrm{B}}T)$—which measures the deviation of electrolyte from ideal gas pressure—is provided by the virial equation [12, 40, 49]. For the case of a binary mixture of components i and j and pairwise additive, density-independent pair potentials, it can be expressed by

$$\phi_v(\rho) = 1 - \frac{\pi}{3}\rho \sum_{i,j} \int_0^\infty g_{ij}(r;\rho)\frac{\mathrm{d}\beta V_{ij}(r)}{\mathrm{d}r} r^3\,\mathrm{d}r, \qquad (7)$$

Table 1. Ion–water oxygen (o) LJ parameters and charges [43–45] and SPC/ E water parameters [24].

Ion	σ_{io} (nm)	ϵ_{io} (kJ mol^{-1})	Charge q/e
Li^+	0.2337	0.6700	+1
Na^+	0.2876	0.5216	+1
K^+	0.3250	0.5216	+1
Cs^+	0.3526	0.5216	+1
Cl^-	0.3785	0.5216	−1
I^-	0.4168	0.5216	−1
SPC/ E			
O	0.3169	0.6500	−0.8476
H	—	—	+0.4238

involving the infinite-dilution pair force $\mathrm{d}V_{ij}(r)/\mathrm{d}r$, while the $g_{ij}(r;\rho)$ has to be evaluated at the density considered. The virial route is *not* exact for an actual three-component case such as a simple salt in water, as many-body contributions to the ion–ion interaction $V_{ij}(r)$ for nonzero densities and multiplet interactions are not considered. It has been demonstrated, however, that those contributions can be quantitatively corrected by taking into account the density dependence of the water dielectric constant $\epsilon(\rho)$ [20, 21, 37]: the long-ranged Coulomb part in the pair potential $V_{ij}(r)$ has to be altered by using $\epsilon(\rho)$ instead of the limit $\epsilon(0)$. The corrected pair potential thus reads [20, 21]

$$\tilde{V}_{ij}(r;\rho) = V_{ij}(r) - \frac{z_i z_j}{r}\left[\lambda_{\mathrm{B}}(0) - \lambda_{\mathrm{B}}(\rho)\right], \qquad (8)$$

which is now implicitly dependent on ρ and has to be used in equation (7) instead. This correction has been validated for concentrations $\rho \lesssim 2$ M by comparing to the exact but computationally more involved compressibility route [37], showing that triplet and higher order ionic interactions are apparently less important.

The necessary input parameter $\epsilon(\rho)$ can be directly calculated from explicit-water MD simulations [37] and is compared to experiments in figure 2. In the salt-free case the dielectric constant is $\epsilon(0) = 72 \pm 1$ for the SPC/ E water model, consistent with the literature value [57], and smaller than $\epsilon(0) = 78.4$ for real water at $T = 298$ K. All salts investigated decrease the dielectric screening of water while, for larger salt concentrations $\rho \gtrsim 0.5$ M, the decrease quantitatively depends on salt type. For densities $\rho \lesssim 2$ M the functional form of $\epsilon(\rho)$ can be fitted reasonably well with the expression $\epsilon(\rho) = \epsilon(0)/[1 + A\rho]$, with $A = 0.31$, 0.27, 0.24, 0.23, and 0.34 l mol^{-1} for LiCl, NaCl, KCl, CsCl, and NaI, respectively. The results for the relative decrease of $\epsilon(\rho)$ with salt type and concentration are in very good agreement with the experimental measurements [50–56] for concentrations up to $\rho \simeq 1$ M.

Figure 3 shows the osmotic coefficients obtained from the virial route (7) and correction (8) using the same salt types for which the short-ranged potentials $V_{ij}^{\mathrm{sr}}(r)$ are displayed in figure 1. The experiments and simulations are in qualitative agreement for the chloride salts, for LiCl and KCl almost quantitative. The MD result for NaI does not reproduce the experimental order, pointing to a suboptimal combination of

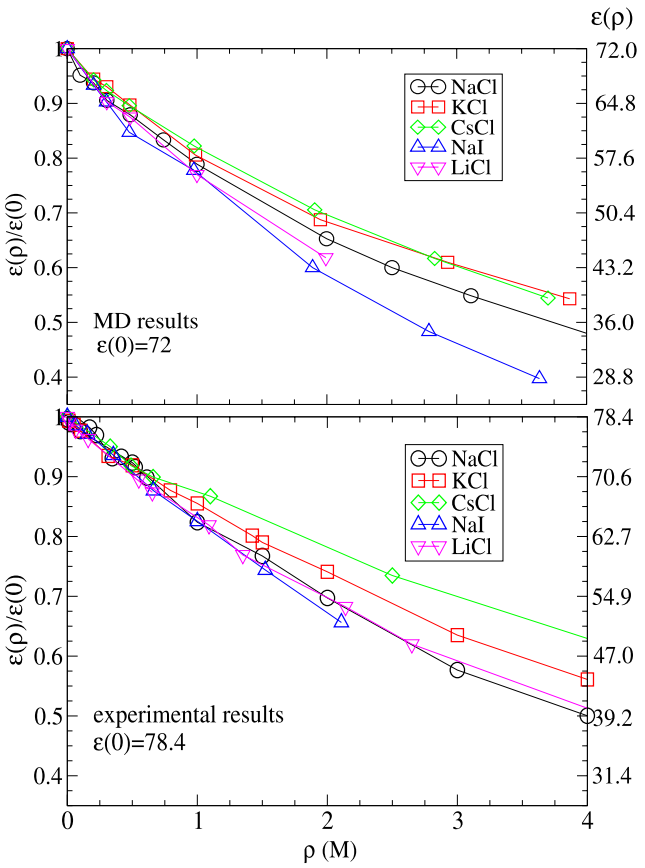

Figure 2. (Color online) Relative water dielectric constant $\epsilon(\rho)/\epsilon(0)$ versus salt concentration ρ from explicit-water MD simulations (top) [37] and experiments [50–56] (bottom). Data points are depicted by symbols while lines are guides to the eye. The labels at the right vertical axes show the absolute $\epsilon(\rho)$ values.

force field parameters. It was pointed out early in the literature that osmotic coefficients are quite sensitive to the particular form of the infinite-dilution pair potential [26]. The qualitative trend observed in the short-ranged pair potentials $V_{ij}^{\mathrm{sr}}(r)$, however, is fully reflected by the osmotic coefficients: NaI and LiCl which feature a weak contact pair formation, have the highest osmotic coefficients of all salts considered. The larger the cation gets, the smaller the osmotic coefficient becomes, indicating less osmotic pressure and thus more attraction in solution. The detailed analysis of all contributions to the osmotic pressure shows that the ion specificity of ϕ up to a $\simeq$2 M concentration is dominated by the form of the cation–anion short-ranged pair potential only [37].

This section has exemplified the tight relation between water-mediated electrolyte structure (cf figure 1), electrolyte-induced water polarization (cf figure 2), and ion specific bulk thermodynamics (cf figure 3) which can only be understood by fully considering the synergetic effects between the electrolyte and its solvent environment. The MD simulation can reproduce experimental trends and gives molecular understanding, while the ionic force fields have to be optimized for a quantitative prediction/reproduction of experimental results.

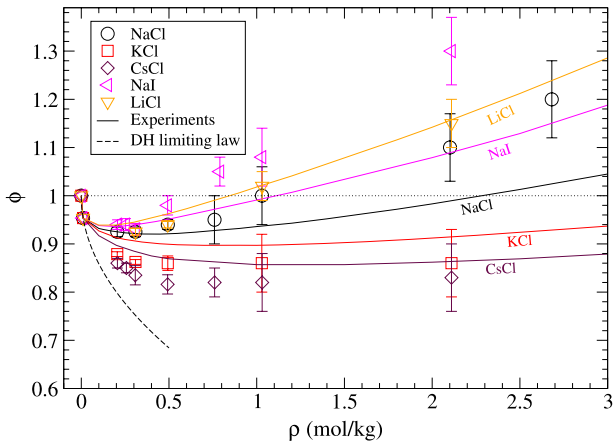

Figure 3. (Color online) The osmotic coefficient ϕ versus salt concentration ρ (in mol kg^{-1}) from the virial route (7) (symbols) using MD-derived pair potentials compared to experimental values (lines). The DH limiting law [8, 58] is also shown (black dashed line).

3. Ion specificity at simple interfaces

So far we have discussed ion specificity in the bulk. Ion specific effects, however, are most often concerned with interfacial behavior which exhibits similarly complex connections between microscopic hydration and specific macroscopic thermodynamics. The question about the relation between ion specific effects in bulk (exemplified by the osmotic coefficient) and ion specificity at surfaces immediately appears.

The classical Hofmeister effect describes the interaction between two proteins as a function of salt type and salt concentration [7]. Let us for the sake of simplicity assume that the two interacting proteins are identical. To a first approximation their interaction can be separated into contributions arising from electrostatic and depletion/adsorption effects. Let us first confine ourselves to neutral surfaces: if the surface repels cations and anions with comparable strength, the interfacial tension will go up and consequently a rather short-ranged attraction will be felt as the surfaces get in close contact. This is commonly denoted as depletion-induced attraction [59]. Conversely, if the surface attracts cations and anions with similar strength, the interfacial tension goes down and a short-ranged repulsion between the surfaces will result; this corresponds to adsorption-induced repulsion. If, on the other hand, a surface interacts differently with anions and cations, in addition to depletion/adsorption interactions for short distances an effective surface charge builds up which will lead to quite long-ranged electrostatic repulsion between similar surfaces [33]. All these effects can be quite conveniently classified by looking at first at a single surface.

Let us consider the simplest surface that shows ion specific adsorption, namely the water–air interface, which can also be considered a model of a flat hydrophobic interface. Previous studies have shown that iodide ions do *adsorb* at the air–water interface [2, 3, 60], in strong contrast with the traditional (continuum) view according to which charges are repelled from low dielectric regions [61]. We present MD

simulation results for the pmf between a single ion and the air–water interface calculated using umbrella sampling [62] in SPC/ E water with nonpolarizable ions in the Gromacs package [63]. In figure 4(a) we plot the pmfs for the simple ions Na^+, K^+, Cl^-, Br^-, and I^-. All ions show roughly the same repulsion, apart from the largest ion iodide which is attracted to the interface. The trend is very similar to the pmfs obtained by previous studies [2, 60] using polarizable force fields for water and ions, though in the present case the polarizability is not included. The LJ parameters for this particular example, however, are systematically optimized on the basis of experimental thermodynamic single-ion data [30] and are $\sigma_{io} = 2.70$ nm and $\epsilon_{io} = 0.65$ kJ mol^{-1} for Na^+, $\sigma_{io} = 3.03$ nm and $\epsilon_{io} = 0.65$ kJ mol^{-1} for K^+, $\sigma_{io} = 3.78$ nm and $\epsilon_{io} = 0.52$ kJ mol^{-1} for Cl^-, $\sigma_{io} = 4.00$ nm and $\epsilon_{io} = 0.37$ kJ mol^{-1} for Br^-, $\sigma_{io} = 4.25$ nm and $\epsilon_{io} = 0.32$ kJ mol^{-1} for I^-. Thus, we can safely state that polarizable force fields are not necessary for observing an iodide attraction to a hydrophobic interface in agreement with other simulation studies [64]. In contrast to the continuum picture, it transpires that the larger the ion (the weaker the ion charge density) the more strongly the ion is pushed to the hydrophobic interface [65]. Figure 4(b) shows a typical simulation snapshot of iodide in the pmf minimum: although charged, it has partly lost its hydration shell. In this view, the large iodide renders itself a hydrophobic entity rather than a hydrophilic one.

How can the putative surface affinity of certain ions be tested experimentally? The direct measurement of surface ion concentrations is difficult to perform, although there are experimental hints of a relatively high interface propensity of iodide [66]. Analogously to the case for osmotic coefficients in the bulk, integrated knowledge is available from surface tension data, for which, on the other hand, simulations are cumbersome. We employ here a multi-scale modeling approach, where the pmfs obtained from MD simulations are fed into a coarse-grained description on the Poisson–Boltzmann (PB) mean-field level [6]. The basic idea is similar to that of the extraction of the short-ranged potential acting between ions in bulk solution: once the short-ranged, solvent-mediated interaction is known, the long-ranged Coulombic interactions can be separately added. Combining the Poisson equation with the Boltzmann equation, one obtains the celebrated PB equation

$$\epsilon_0 \frac{\mathrm{d}}{\mathrm{d}z}\epsilon(z)\frac{\mathrm{d}}{\mathrm{d}z}\Psi(z) = -\sum_i q_i \rho_i(\infty)\exp[-\beta q_i \Psi(z) - \beta V_i^{\mathrm{w}}(z)] \tag{9}$$

where $\epsilon(z)$ is the relative dielectric constant profile as a function of the distance z from the surface and which we take to be constant. $\Psi(z)$ is the local electrostatic potential profile, q_i is the charge of the ith ion, $\rho_i(\infty)$ is its bulk (or reservoir) concentration, and $V_i^{\mathrm{w}}(z)$ is the wall–ion pmf of the ith ion. The concentration profile of the ith ion follows as

$$\rho_i(z) = \rho_i(\infty)\exp[-\beta q_i \Psi(z) - \beta V_i^{\mathrm{w}}(z)]. \tag{10}$$

The surface excess of ionic species i is defined as

$$\Gamma_i = \int_{-\infty}^{z_{\mathrm{G}}} \rho_i(z)\,\mathrm{d}z + \int_{z_{\mathrm{G}}}^{\infty} [\rho_i(z) - \rho_i(\infty)]\,\mathrm{d}z \tag{11}$$

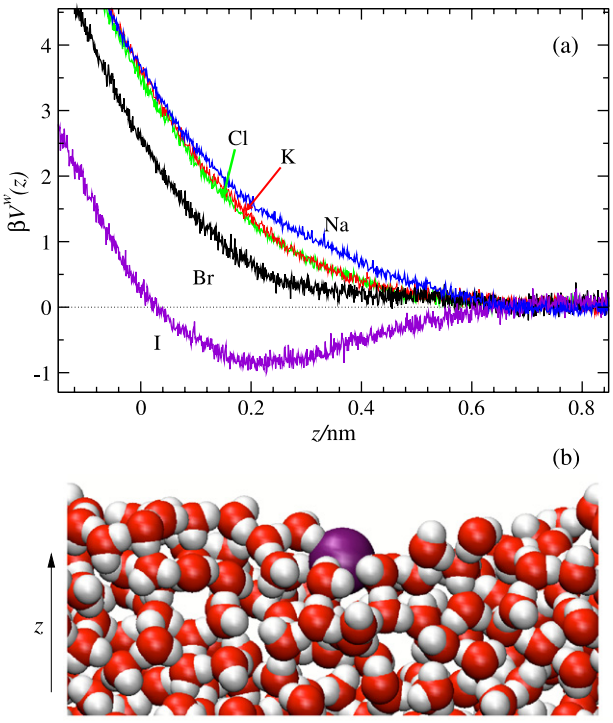

Figure 4. (Color online) (a) Potentials of mean force for simple ions at a distance z from the air–water interface. There is a clear ordering of the potentials of mean force: the largest anion, iodide, is attracted to the interface; the smaller anions and cations are increasingly repelled from the interface with decreasing ion size. (b) Simulation snapshot of an iodide anion (purple sphere) at the air–water interface.

where the Gibbs-dividing-surface position z_{G} is defined by the requirement that the surface excess of water itself vanishes. Finally, the Gibbs equation relates the surface tension change due to added solute to the concentration integral over the surface excess,

$$\Delta\gamma = -k_{\mathrm{B}}T\int_0^{\rho}\sum_i \Gamma_i(\rho')/\rho'\,\mathrm{d}\rho'. \tag{12}$$

In figure 5 we show the surface tension increment of 1 M of sodium halide solutions compared to experimental data. The experimental trend is nicely reproduced; the larger the anion, the smaller the surface tension increment, corroborating the observed enhanced affinity of iodide to a hydrophobic interface. Interestingly, the adsorption strength of iodide seems to be overestimated by the simulations implying that the actual surface affinity of iodide may be an even smaller effect. On the other hand, the inclusion of a position-dependent dielectric constant and bulk correlations in this mean-field analysis may improve agreement.

Let us now turn to electrolyte solutions confined between two simple *charged* surfaces. The surfaces in our example are modeled by a solid-like assembly of atomistic LJ spheres in a close-packed hexagonal lattice arrangement which is harmonically restrained; see the snapshot in figure 6. The LJ length is chosen such that the atoms have the size of a methyl group $\sigma_{ii} = 0.3905$ nm [63]. The energy $\epsilon_{ii} = 1.024 k_{\mathrm{B}}T$ is chosen such that the contact angle of paraffin of $\simeq$112° is

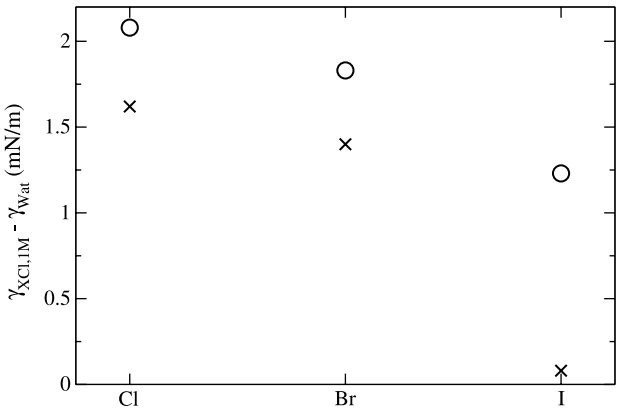

Figure 5. The difference in surface tension $\Delta\gamma$ of a 1 M sodium halide solution and pure water. The circles show experimental data from [10]; the crosses are our predictions obtained from equation (12) with the pmfs of sodium and the halides shown in figure 4(a). The qualitative trend in the experimental data is reproduced; the surface tension increase becomes smaller for the series Cl–Br–I.

reproduced, calculated by a simple mean-field integration over the interactions between the solid and the liquid [67]. The ion parameters are those of Dang as used in the bulk simulations in section 2. The two confining surfaces are oppositely charged by assigning every atom in the first solid layer a partial charge of q, leading to a surface charge density of $\sigma = nq/(L_x L_y)$. Typically $n = 120$ surface atoms are involved, the lateral wall sizes are $L_x = L_y = 4.2$ nm, and the charge is $q < e$.

Before we turn to the charged walls, in figure 7 we plot the wall–ion pmfs at infinite dilution for Na^+, Cl^- and I^- for the neutral walls, $\sigma = 0$. Although we are using slightly different ion parameters than in the liquid–vapor interface system and the hydrophobic interface is chemically different and solid, Na^+ is still repulsive and the pmf of I^- again shows a clear minimum and is attracted to the surface. This clearly demonstrates the insensitivity of this trend to the particular force field and chemical nature of the hydrophobic surface. Even in simulations of more realistic molecular surfaces binding of iodide to the interface has been observed [68]. Interestingly, this association mediates an iodide-assisted attraction between nonpolar faces of proteins, lowering the protein's second virial coefficient in agreement with experiments [36].

Figure 6 displays the density profiles for Na^+ and I^- between two *charged* solid-like walls in a surface-to-surface distance of $L = 4$ nm for a salt area concentration (number of salt pairs per area) $\tau = 2.2$ nm^{-2} which roughly corresponds to a 0.9 M bulk solution. The surface charge density in this example is $\sigma = 0.11\ e$ nm^{-2}. We observe the anticipated trend that the positive sodium is attracted to the negative surface (left) and iodide to the positive one (right). The double-layer profiles for anions and cations, however, are strongly asymmetric due to the individual intrinsic interactions with the hydrophobic wall as discussed before. Obviously, the density profiles have much more structure than calculations in the primitive model with only hard-core interactions between surface and ions; see e.g., [6, 42]. Consequently, specific

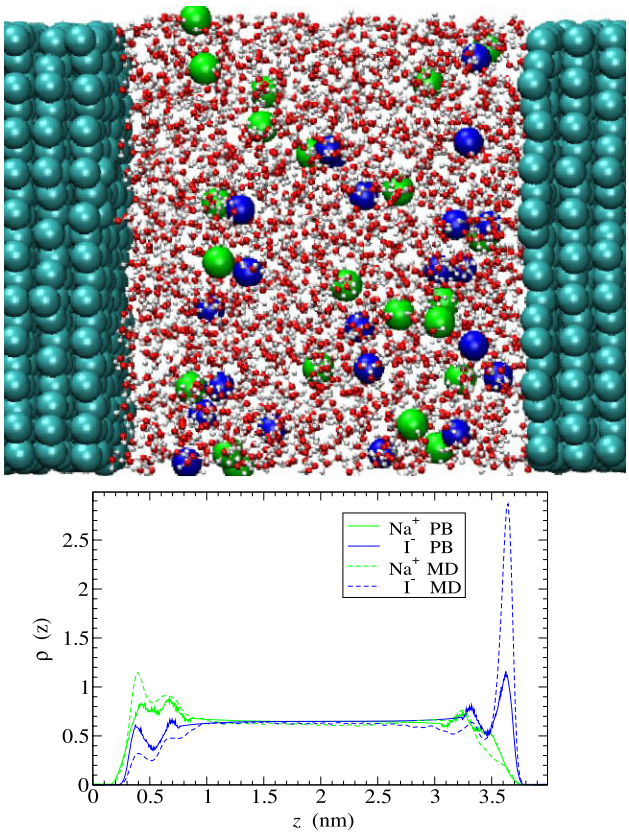

Figure 6. (Color online) Top: illustrative MD snapshot of sodium (blue) and iodide (green) ions and water (red–white) between two oppositely charged walls. The surface charge density in this example is $\sigma = 0.11\ e$ nm^{-2}. The left wall is negatively charged. Bottom: corresponding ion density profiles for NaI electrolyte solutions from explicit-water MD simulations (dashed lines). The ion density profiles are compared to the solution of the Poisson–Boltzmann equation (9) (solid lines).

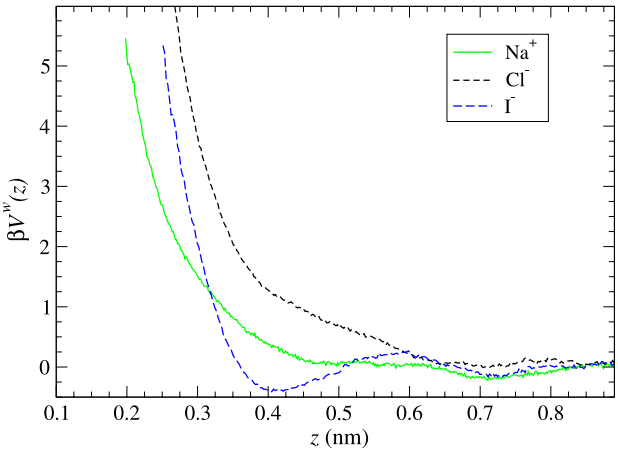

Figure 7. (Color online) Potentials of mean force for Na^+, Cl^-, and I^- at a distance z from a neutral carbon-like surface; cf figure 6.

ion adsorption clearly affects the osmotic pressure and mutual surface interaction between charged surfaces which should be applicable also to macromolecular biological entities [36].

In the next step we try to reproduce the profiles by the standard PB approach (9) using a constant dielectric constant

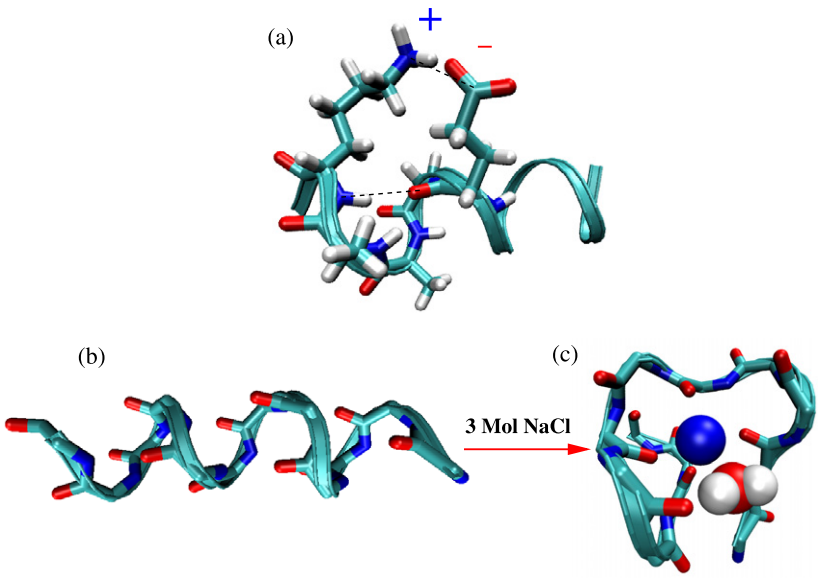

Figure 8. (Color online) MD simulation snapshots of a peptide 12 amino acids long. Water molecules are omitted for clarity. (a) Without salt, the helical fold is locally stabilized by E^{-}–K^{+} salt bridges (only E and K side chains at sequence positions 2 and 6 are shown, respectively). (b) The equilibrium helical configuration shifts to (c) a coil-like structure after addition of 3 M NaCl [5]. In the denatured state, sodium (blue sphere) and water molecules (red–white spheres) can hydrogen bond to the peptide backbone on a long, nanosecond timescale. Side chains are omitted for clarity in (b) and (c).

$\epsilon = 53$, which is the value of a 0.9 M NaCl solution in SPC/ E water [37]. As can be seen, the main features of the profiles, such as peak positions and density in the slab center, are reproduced by the PB approach. On the other hand it is not capable of accurately resolving the fine oscillating structure near the walls. An improved version of PB for concentrated electrolyte solutions certainly needs to account for a local dielectric constant $\epsilon(z)$ and steric (excluded volume) effects [69]. On a more sophisticated level, the water-mediated ion–ion correlations (cf figure 1) have to be included in a nonlocal way [70]. Other primitive model calculations, e.g., as in integral equation theory, may benefit from inclusion of MD generated ion–wall pmfs in the description of double layers [6, 42].

Let us finally note that some of the ion binding effects on solid surfaces have been experimentally observed by different techniques such as electro-osmosis [71], thin-film pressure-balance studies [72], single-molecule desorption studies [73], capacitance studies [74], and surface-sensitive field-effect setup studies [75]. Biological surfaces exhibit an even higher level of complexity due to their heterogeneous chemical and geometrical nature, featuring patterns of hydrophobic, polar, and highly charged surface groups. The investigation of the structural stability of a small biomolecule follows in the next section.

4. Ion specific action on the secondary structure of biomolecules

Having exemplified ion specificity in bulk and at simple interfaces, in this section we discuss the specific action of salt on the structure of a single helical peptide that serves as a simple but realistic model for a small biological protein. The sequence of the peptide is Ace–AEAAAKEAAAKA–Nme, where A is a hydrophobic alanine, E denotes a glutamic acid (Glu) with a side chain terminated by a negatively charged carboxylate group, and where K denotes a lysine (Lys) which has a side chain terminated by a positive nitrogen amide group. The amino acid alanine is known to have a high intrinsic helix forming affinity and this peptide additionally features two stabilizing E–K ionic salt bridges, which leads to strong helix formation [76].

The peptide and solution structure in explicit-water electrolyte environments (NaCl, KCl, and NaI) at zero and large salt concentrations (3–4 M) is investigated using all-atom MD from the AMBER package [77] with explicit resolution of the water and ions. The latter are modeled by nonpolarizable Dang ions with parameters as in table 1. It is found that without salt, the peptide displays on average 71% α-helical structure but destabilizes with the addition of NaCl where the average helicity is $\simeq$30%, both numbers in agreement with experiments of a somewhat longer version [76]. NaI is found to have more denaturation potential than NaCl (helicity $\simeq$20%), while the potassium salt hardly shows any influence (helicity: $\simeq$65%). NaI is indeed known to be a strong denaturant [4].

The MD simulations [5] reveal that the helical structure is indeed partly stabilized by ('$i+4$') EK salt bridges between the Lys and Glu side chains, as illustrated in figures 8(a) and (b). As an important secondary effect, a concomitant backbone shielding mechanism is observed where secondary-structure stabilizing hydrogen bonds between the polar backbone carbonyls (negative partial charge) and nitrogens (positive partial charge) are protected from solvent interactions. Adding NaCl or NaI, however, destabilizes salt-bridge formation and subsequently the helix by specific binding of Na^{+} to the carboxylate head groups. Additionally specific binding of

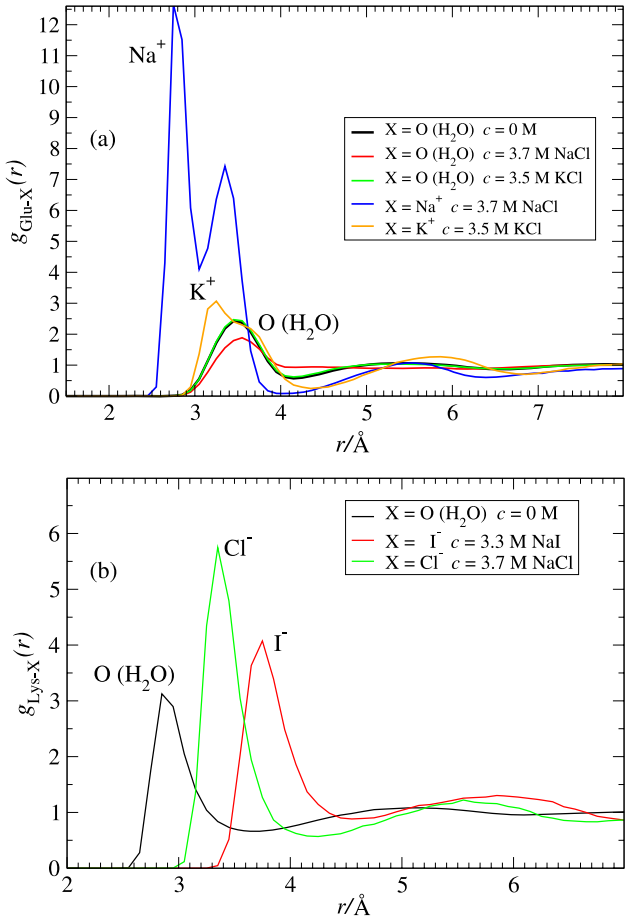

Figure 9. (Color online) (a) Radial distribution function (rdf) $g_{\mathrm{Glu-X}}(r)$ between the carboxylate carbon of the Glu side chains and X, where X = O (water oxygen), Na^+, or K^+, plotted for no salt ($c = 0$) and NaCl and KCl at concentrations $c \simeq 3$–4 M. (b) rdf $g_{\mathrm{Lys-X}}(r)$ between the nitrogen of the Lys side chain and X, where X = O (water oxygen), Cl^- or I^-.

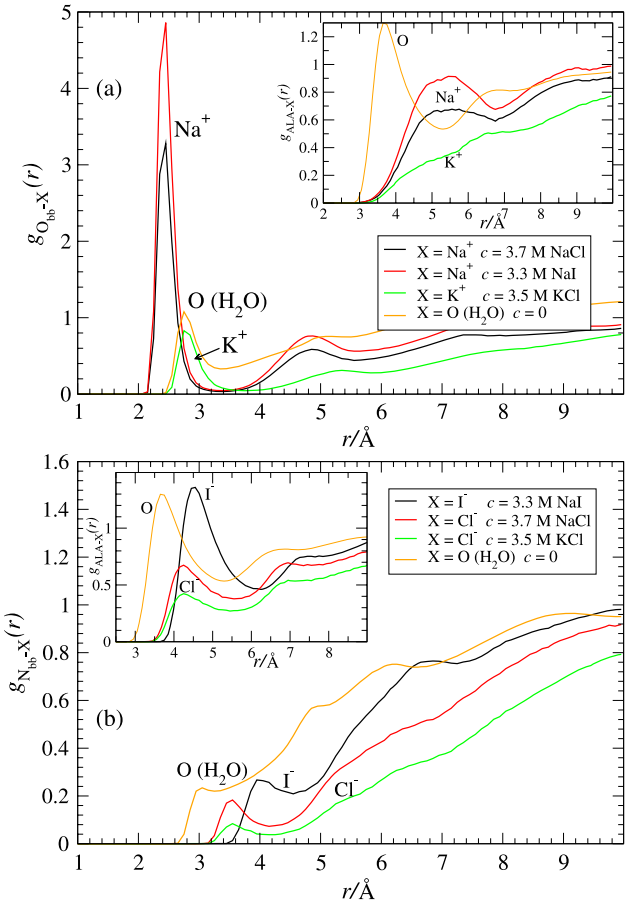

Figure 10. (Color online) (a) Radial distribution function (rdf) $g_{\mathrm{O_{bb}-X}}(r)$ between the backbone oxygen and X, where X = Na^+, K^+, or water oxygen (O) plotted for different salts; see the legend. Inset: rdf $g_{\mathrm{ALA-X}}(r)$ between alanine side chains and X. (b) rdf $g_{\mathrm{N_{bb}-X}}(r)$ between the backbone nitrogen and X, where X = Cl^-, I^-, or water oxygen (O) for different salts; see the legend. Inset: rdf $g_{\mathrm{ALA-X}}(r)$ between alanine side chains and X.

sodium and iodide to the backbone carbonyls and hydrophobic alanine side chains, respectively, is observed, disturbing intra-backbone hydrogen bonds. The specific ion binding is detailed in figures 9 and 10 where radial distribution functions (rdfs) between bulk ions and selected peptide groups are shown.

In figure 9(a) the rdf of water and ions around the Glu head group are shown. Strikingly, and observable from the contact peak, there is strong affinity of sodium to the carboxylates over potassium as has been found in previous experimental studies and quantum mechanical calculations [78, 79]. The rdf of potassium on the other hand is comparable in magnitude to that of the water oxygen; to quantify, the coordination number of species i in the first carboxylate solvation shell is estimated with

$$N_i(r_c) = \rho_i \int_0^{r_c} \mathrm{d}^3 r g(r), \qquad (13)$$

where $r_c = 4.3$ Å is chosen to be the extension of the first solvation shell and ρ_i is the number density of species i. While in the salt-free case 8–9 water molecules directly solvate the carboxylate, ∼2 of them are replaced on average by sodium ions in the NaCl solution, indicating a strong specific binding of sodium weakening the salt bridge. In KCl on average only ∼0.5K^+ ions replace water molecules, showing that potassium is much weaker in breaking direct or indirect salt bridges. The distributions of water and anions around the Lys nitrogen are plotted in figure 9(b): Cl^- is preferred over I^- as could have been expected from electrostatic considerations, i.e., there is a stronger attraction with larger ion charge density. Calculating coordination numbers as above, however, reveals that only on average ∼0.3 chloride ions are able to replace a water molecule in the water solvation shell, much less effective in replacing water than sodium around the carboxylates. Thus, the strong affinity of sodium to the carboxylates decreases the probability of forming direct or indirect salt bridges, and thereby decreases helix stability.

Similar specific binding can also be detected between ions and the backbone oxygens and nitrogen atoms: examples for the cation and anion rdfs are plotted in figures 10(a) and (b), respectively. A strong attraction of sodium to the carbonyl oxygens is observed in striking contrast to a weak affinity of potassium. The anions, however, interact with the backbone even more weakly; cf figure 10(b). Interestingly, iodide shows

the highest first peak compared to chloride, conversely to its interaction with the Lys head group (see figure 9(b)), where $Cl^- > I^-$. Related to this, the strong affinity of sodium to the backbone is even enhanced in the presence of iodide. We argue that these effects have two origins: firstly, the bulk osmotic pressure (or activity) of NaI is larger than that of NaCl at the same concentration (cf figure 3); in other words, transferring a sodium–iodide pair from a NaI solution to a reference solution costs less energy than doing so from NaCl. Secondly, as demonstrated in section 3 and previous literature [2, 31], the relatively large anions are attracted to hydrophobic surfaces. To inspect this hypothesis for our (partly nonpolar) peptide, the rdfs between the carbon atom in the alanine side chain and cations or anions are shown in the insets to figures 10(a) and (b), respectively. Iodide has indeed the strongest affinity to the nonpolar side chains from all ions considered, giving rise to a relatively high affinity to the protein surface. These findings agree with the perspective that the iodide propensity for nonpolar surfaces may indeed impact protein stability [2, 36, 68, 80], a mechanism also proposed for other large ions such as guanidium [81].

Further inspection of MD trajectories for NaCl and NaI reveals that the strong interaction of sodium with the backbone carbonyls can result in intriguingly long-lived denatured peptide configurations where sodium is bound and involved in the peptide structure, as shown in figure 8(c). The central part of the peptide loops around a single sodium ion, thereby binding it with 3–4 backbone oxygens. Sometimes an additional water molecule is captured by the backbone–ion complex and binds. These states are surprisingly stable on a long 10–20 ns timescale. No such long-lived states involving potassium or anions are observed.

In summary, Na^+ has a much stronger affinity to side chain carboxylates and backbone carbonyls than K^+, thereby weakening salt bridges and secondary-structure hydrogen bonds. At the same time the large I^- has a considerable affinity to the nonpolar alanine in line with recent observations of a large propensity of I^- to adsorb to simple hydrophobes, and thereby 'assists' Na^+ in its destabilizing action. Thus, the protein secondary-structure stability in electrolyte solutions is determined by complex synergetic binding events, in particular a delicate interplay between peptide–peptide and ion–peptide interactions, in which both hydrophobic and hydrophilic interactions are essential. A few of these mechanisms can be understood from the interactions in simpler bulk or interfacial systems, as exemplified in the previous sections.

5. Concluding remarks

Ion specificity results from a subtle competition between ion hydration, i.e., binding and polarization of water molecules in bulk, ion pairing, and the interaction of ions with nonpolar or polar groups at surfaces. The combination of explicit-water MD simulations and liquid state theory enables us to bridge microscopic structural data and experimentally measurable quantities in electrolyte systems, allowing a molecular understanding of ion specific effects. While the accuracy of the underlying classical force field in the MD is crucial for capturing the sensitive hydration effects, and force field optimization is still work in the process, recent MD studies have clearly demonstrated their usefulness in revealing Hofmeister effects in a variety of systems. The observed hydration complexity and the collection of different binding effects (in bulk, at hydrophilic versus hydrophobic surfaces, etc) make it hard to believe that on a coarser level, ion specificity can be modeled using standard primitive models with effective hard-sphere interactions for the ions only. We expect that structural input from molecular approaches will play an increasingly important role, e.g., in modified PB or integral equation approaches, for capturing the observed complexity.

Acknowledgments

JD and IK are grateful to the Deutsche Forschungsgemeinschaft (DFG) for support within the Emmy-Noether-Program. We thank the German Arbeitsgemeinschaft industrieller Forschungsvereinigungen Otto von Guericke e.V. (AiF) in the framework of the project 'Simulation and prediction of salt influence on biological systems' and the Leibniz-Rechenzentrum (LRZ) München for computing time on HLRB II.

References

[1] Alberts B, Johnson A, Lewis J, Raff M, Roberts K and Walter P 2002 *Molecular Biology of the Cell* (New York: Garland Science)
[2] Jungwirth P and Tobias D J 2006 *Chem. Rev.* **106** 1259
[3] Tobias D J and Hemminger J C 2008 *Science* **319** 1197
[4] Baldwin R L 1996 *Biophys. J.* **71** 2056
[5] Dzubiella J 2008 *J. Am. Chem. Soc.* **130** 14000
[6] Durand-Vidal S, Simonin J-P and Turq P 2002 *Electrolytes at Interfaces* vol 1 *Progress in Theoretical Chemistry and Physics* (Dordrecht: Kluwer–Academic)
[7] Kunz W, Nostro P L and Ninham B W 2004 *Curr. Opin. Colloid Interface Sci.* **9** 1 (special issue)
[8] Debye P and Hückel E 1923 *Phys. Z.* **24** 185
[9] Robinson R A and Stokes R H 2002 *Electrolyte Solutions* 2nd edn (New York: Dover)
[10] Barthel J M G, Krienke H and Kunz W 1998 *Physical Chemistry of Electrolyte Solutions: Modern Aspects* (Berlin/Darmstadt: Springer/Steinkopff)
[11] Neal B L, Asthagiri D and Lenhoff A M 1998 *Biophys. J.* **75** 2469
[12] Enderby J E and Neilson G W 1981 *Rep. Prog. Phys.* **44** 593
[13] Rajamani S, Ghosh T and Garde S 2004 *J. Chem. Phys.* **120** 4457
[14] Soper A K and Weckström K 2006 *Biophys. Chem.* **124** 180
[15] Karplus M and McCammon J A 2002 *Nat. Struct. Mol. Biol.* **9** 646
[16] Zhu S-B and Robinson G W 1992 *J. Chem. Phys.* **97** 4336
[17] Lyubartsev A P and Laaksonen A 1995 *Phys. Rev.* E **52** 3730
[18] Lyubartsev A P and Laaksonen A 1997 *Phys. Rev.* E **55** 5689
[19] Uchida H and Matsuoka M 2004 *Fluid Phase Equilib.* **219** 49
[20] Hess B and Holm C 2006 *Phys. Rev. Lett.* **96** 147801
[21] Hess B, Holm C and van der Vegt N 2006 *J. Chem. Phys.* **124** 164509
[22] Gavryushov S 2006 *J. Phys. Chem.* B **110** 10888
[23] Gavryushov S and Linse P 2006 *J. Phys. Chem.* B **110** 10878
[24] Berendsen H J C, Grigera J R and Straatsma T P 1987 *J. Phys. Chem.* **91** 6269

[25] Ramanathan P S and Friedman H L 1971 *J. Chem. Phys.* **54** 1086
[26] Pettitt B M and Rossky P J 1986 *J. Chem. Phys.* **84** 5836
[27] Dang L X, Pettitt B M and Rossky P J 1992 *J. Chem. Phys.* **96** 4046
[28] Patra M and Karttunen M 2004 *J. Comput. Chem.* **25** 678
[29] Joung I S and Cheatham T E III 2008 *J. Phys. Chem.* B **112** 9020
[30] Horinek D, Mamatkulov S and Netz R R 2009 *J. Chem. Phys.* **130** 124507
[31] Horinek D and Netz R R 2007 *Phys. Rev. Lett.* **99** 226104
[32] Thomas A S and Elcock A H 2007 *J. Am. Chem. Soc.* **129** 14887
[33] Horinek D, Serr A, Bonthuis D J, Boström M, Kunz W and Netz R R 2008 *Langmuir* **24** 1271
[34] Fedorov M V, Goodman J M and Schumm S 2009 *Chem. Commun.* **8** 896
[35] Lund M, Vrbka L and Jungwirth P 2008 *J. Am. Chem. Soc.* **130** 11582
[36] Lund M, Jungwirth P and Woodward C E 2008 *Phys. Rev. Lett.* **100** 258105
[37] Kalcher I and Dzubiella J 2009 *J. Chem. Phys.* **130** 134507
[38] Mayer J E 1968 *Equilibrium Statistical Mechanics* (Oxford: Pergamon)
[39] McMillan W G and Mayer J E 1945 *J. Chem. Phys.* **13** 276
[40] Hansen J P and McDonald I R 1986 *Theory of Simple Liquids* 2nd edn (London: Academic)
[41] Perkyns J and Pettitt B M 1992 *J. Chem. Phys.* **97** 7656
[42] Greberg H and Kjellander R 1998 *J. Chem. Phys.* **108** 2940
[43] Dang L X 1992 *J. Chem. Phys.* **96** 6970
[44] Dang L X and Garrett B C J 1993 *J. Chem. Phys.* **99** 2972
[45] Dang L X 1995 *J. Am. Chem. Soc.* **117** 6954
[46] Collins K D 1997 *Biophys. J.* **65** 65
[47] Collins K D 2004 *Methods* **34** 300
[48] Lyklema J 2009 *Chem. Phys. Lett.* **467** 217
[49] Rasaiah J C and Friedman H L 1968 *J. Chem. Phys.* **48** 2742
[50] Wei Y-Z, Chiang P and Sridhar S 1992 *J. Chem. Phys.* **96** 4569
[51] Lyashchenko A K and Zasetsky A Y 1998 *J. Mol. Liq.* **77** 61
[52] Loginova D V, Lileev A S and Lyashchenko A K 2006 *Russ. J. Phys. Chem.* **80** 1626
[53] Buchner R, Hefter G T and Barthel J 1994 *J. Chem. Soc. Faraday Trans.* **90** 2475
[54] Nörtemann K, Hilland J and Kaatze U 1997 *J. Phys. Chem.* A **101** 6864
[55] Wachter W, Kunz W, Buchner R and Hefter G 2005 *J. Phys. Chem.* A **109** 8675
[56] Barthel J, Buchner R and Münsterer M 1995 *Electrolyte Data Collection* part 2, vol 12 (Frankfurt: Dechema)
[57] Kusalik P G and Svishchev I M 1994 *Science* **265** 1219
[58] Barrat J and Hansen J P 2003 *Basic Concepts for Simple and Complex Liquids* 1st edn (Cambridge: Cambridge University Press)
[59] Allahyarov E, D'amico I and Löwen H 1998 *Phys. Rev. Lett.* **81** 1334
[60] Chang T-M and Dang L X 2006 *Chem. Rev.* **106** 1305
[61] Jackson J D 1999 *Classical Electrodynamics* 3rd edn (New York: Wiley)
[62] Allen M P and Tildesley D J 1987 *Computer Simulation of Liquids* (Oxford: Clarendon)
[63] Lindahl E, Hess B and van der Spoel D 2001 *J. Mol. Mod.* **7** 306
[64] dos Santos D J V A, Müller-Plathe F and Weiss V C 2008 *J. Phys. Chem.* C **112** 19431
[65] Huang D M, Cottin-Bizonne C, Ybert C and Bocquet L 2008 *Langmuir* **24** 1442
[66] Petersen P B, Johnson J C, Knutsen K P and Saykally R J 2004 *Chem. Phys. Lett.* **397** 46
[67] Rowlinson J and Widom B 1982 *Molecular Theory of Capillarity* (Oxford: Oxford University Press)
[68] Lund M, Vácha R and Jungwirth P 2008 *Langmuir* **24** 3387
[69] Borukhov I, Andelman D and Orland H 1997 *Phys. Rev. Lett.* **79** 435
[70] Hansen J-P and Löwen H 2000 *Annu. Rev. Phys. Chem.* **51** 209
[71] Schweiss R, Welzel P B, Werner C and Knoll W 2001 *Langmuir* **17** 4304
[72] Ciunel C, Armelin M, Findenegg G H and von Klitzing R 2005 *Langmuir* **21** 4790
[73] Friedsam C, Gaub H E and Netz R R 2005 *Europhys. Lett.* **72** 844
[74] Garcia-Celma J J, Hatahet L, Kunz W and Fendler K 2007 *Langmuir* **23** 10074
[75] Härtl A, Garrido J A, Nowy S, Zimmermann R, Werner C, Horinek D, Netz R R and Stutzmann M 2007 *J. Am. Chem. Soc.* **129** 1287
[76] Marqusee S and Baldwin R L 1987 *Proc. Natl Acad. Sci.* **84** 8898
[77] Case D A 2006 *Software AMBER9.0* University of California, San Francisco
[78] Vrbka L, Jagoda-Cwiklik B, Vácha R and Jungwirth P 2006 *Proc. Natl Acad. Sci.* **103** 15440
[79] Uejio J S, Schwartz C P, Duffin A M, Drisdell W S, Cohen R C and Saykally R J 2008 *Proc. Natl Acad. Sci.* **105** 6809
[80] Kalra A, Tugcu N, Cramer S and Garde S 2001 *J. Phys. Chem.* B **105** 6380
[81] Mason P E, Brady J W, Neilson G W and Dempsey C E 2007 *Biophys. J.* **93** L04